PERGAMON

International Journal of Heat and Mass Transfer 42 (1999) 861–872

International Journal of HEAT and MASS TRANSFER

Coupled heat and mass transfer of a stagnation point flow in a heated porous bed with liquid film evaporation

T. S. Zhao*

Department of Mechanical Engineering, The Hong Kong University of Science and Technology, Clear Water Bay, Kowloon, Hong Kong

Received 7 November 1997; in final form 24 June 1998

Abstract

An analytical solution is presented for the study of coupled heat and mass transfer in a stagnation point flow of air through a heated porous bed with thin liquid film evaporation. The analysis indicates that the coupled heat and mass transfer process in the air stream induced by the evaporation of a thin liquid water film embedded in the porous medium of a given porous material is governed by the Peclet number *Pe*, the Lewis number *Le*, the porosity of the porous bed ϕ, as well as the ambient temperature T_∞ and relative humidity φ of air. It is shown that the heat transfer between the heated plate and the air stream is predominated by the transport of the latent heat associated with the thin liquid film evaporation. The analysis also demonstrates that the air stream with a lower relative humidity, a higher temperature, and a higher Peclet number lead to an increase of heat transfer rate. For the case when $Le > 1$, the mass transfer rate is enhanced while the heat transfer rate is reduced. These findings are of significance for the design of a cross-flow indirect evaporative air cooler.

Nomenclature

A constant in equation (22)
b thickness of porous bed [m]
C constant in equation (7)
C_1, C_2 constants in equation (23)
c_p specific heat [J kg^{-1} K^{-1}]
D mass diffusivity in the plain media [m^2 s^{-1}]
D_m mass diffusivity in the porous media region [m^2 s^{-1}]
h heat transfer coefficient [W m^{-2} °C^{-1}]
h_{fg} latent heat of vaporization [J kg^{-1} K^{-1}]
Ja' modified Jacob number
k stagnation flow strain rate [s^{-1}]
K permeability
Le Lewis number
$\dot{m}_{v,i}$ evaporating flux of water vapor [kg s^{-1}]
Nu Nusselt number
Nu_l latent Nusselt number
Nu_s sensible Nusselt number
Pe_l Peclet number
p_∞ ambient pressure [kg m^{-2}]
q total heat flux [W m^{-2}]
q_l latent heat flux [W m^{-2}]
q_s sensible heat flux [W m^{-2}]
T temperature [°C]
T_i temperature at liquid–gas interface [°C]
T_∞ ambient temperture [°C]
v velocity [m s^{-1}]
w mass fraction of water vapor [kg kg^{-1}]
w_i mass fraction of water vapor at liquid–gas interface [kg kg^{-1}]
w_∞ ambient mass fraction of water vapor [kg kg^{-1}]
W w/w_∞
x, y system coordinates [m]
X, Y dimensionless coordinates.

Greek symbols

α thermal diffusivity [m^2 s^{-1}]
α_m effective thermal diffusivity [m^2 s^{-1}]
γ thermal conductivity ratio of fluid to solid
θ dimensionless temperature
Λ_i constants in equations (27) and (30)
λ thermal conductivity [W m^{-1} °C^{-1}]
λ_m effective thermal conductivity [W m^{-1} °C^{-1}]

* Tel.: 00852 2358 8647; fax: 00852 2358 1543; e-mail: metzhao@ust.hk

0017–9310/98/$—see front matter
PII: S0017–9310(98)00213–0

ρ density [kg m^{-3}]
σ_α α_m/α
σ_D D_m/D
σ_λ λ_m/λ
ϕ porosity
φ relative humidity [%].

Subscripts
i liquid–gas interface
l latent
s sensible.

1. Introduction

Wet surface heat exchangers are widely used in refrigeration, air conditioning, cooling towers and power plant systems. In these heat exchangers, both air and liquid water are used as the cooling media [1]. For instance, in an indirect evaporative cooler heat is transferred from a warm, dry air stream to a cooler, moist air stream through an exchange surface separating the two fluids. These two fluid streams and associated exchange surfaces are usually referred to as primary and secondary, respectively. The secondary surface is wetted by circulating water, so as to evaporatively cool the secondary air in direct contact with water films. In this manner, heat is transferred from primary to secondary air without the introduction of moisture into the primary air stream. In recent years, extensive studies of evaporative cooling systems that include indirect evaporative cooling equipment have been carried out [2]. The primary objective of these studies is to determine the energy savings and peak load reduction potential of the evaporative cooling technology compared to conventional vapor-compression air conditioning. Generally, it was reported that the energy savings of 30–47% can be obtained, depending on local climates. Peterson and Hunn [3] reported peak load reduction of 16%, even in humid climates when indirect evaporative cooling systems are used in small office buildings. However, the major challenge of an indirect evaporating cooling system is to design a high heat and mass transfer rate wet surface heat exchanger, so that an indirect evaporative cooling unit can be more efficient and more compact.

The thermal analysis of a wet surface heat exchanger is inherently complicated because the cooling process involves simultaneous heat and mass transfer at the liquid film–air interface. McClaine-Cross and Banks [4] analyzed the performance of a wet surface heat exchanger by using a one-dimensional mathematical model. They made their calculation for the whole area of the heat and mass transfer plate based on the averaged temperatures and the averaged humidity ratios at entry and exit of the heat exchanger. Another assumption they made was that the plates were completely wet. Their results are 20% higher than the experimental data. A more detailed analysis was carried out by Hsieh and Kettleborough [5] for counterflow heat exchangers and by Kettleborough [6] for crossflow heat exchangers. In both cases the analysis was carried out by considering a single plate and the velocities were assumed to be constant; the computed effectiveness was 14% higher than experimental values. In subsequent studies [7–11], the effects of various physical and structural properties in the evaporative channels on the thermal performance of the unit were widely investigated. Kettleborough [7] derived the heat and mass balance equations for the primary and secondary flows and studied the effect of primary velocity on the cooler performance. However, their theoretical prediction did not agree well with the experimental data by Pescode [11]. Wassel and Mills [8] illustrated a design methodology for a countercurrent falling film evaporative cooler. It was found that narrow flow passages were more effective for the evaporative condenser. Hsu and Lavan [9] used an iterative, column-row, successive over-relaxation technique to solve the governing equations in a cross-flow parallel plate regenerative indirect evaporative cooler. They assumed that the water was locally replenished and the water layer was negligibly thin (no thermal resistance). Erens and Dreyer [10] presented three analytical models, and their results show that the optimum shape of the cooler unit would result in a primary to secondary air velocity ratio of about 1.4, assuming that the primary and the secondary air mass flow rates are the same and that the same plate spacings are used on the primary and secondary sides.

All of the above analyses on the flat wet surface heat exchanger were conducted by assuming that the air stream is a plug flow and the heat transfer coefficient in the wet surface depends on the velocity only. Obviously these assumptions may lead to errors compared with experimental data. Until recently, several analyses on simultaneous heat and mass transfer in the wet surface heat exchanger have been reported. Tsay [1] numerically analyzed a countercurrent-flow wet surface heat exchanger. He compared the heat transfer rates in a wet surface heat exchanger with those obtained in a dry surface heat exchanger, and found that the energy transported across the liquid film was mostly absorbed by the film vaporization process. Yan and Soong [12] presented their numerical solution for convective heat and mass transfer along an inclined heated plate with film evaporation. They studied the inclination angle of the plate on the heat transfer rate of a wet surface heat exchanger. In another paper, Yan [13] also reported the effects of film vaporization on turbulent mixed convection heat and mass transfer in a vertical channel. All these analyses were restricted to the study of the wet surface heat exchanger with flat solid surface. Since the energy transport in a wet surface heat exchanger is dominated by the latent heat transfer through the evaporation of the water

film, it is essential that a large contact area between air and water be obtained. For this reason, corrugated [11] or porous structure can provide a large air–water contact area and thereby increasing wettability and the heat and mass transfer rate. However, the coupled heat and mass transfer process becomes more complicated by the presence of a porous medium. This motivates the present study.

In this paper, we investigate the coupled heat and mass transfer in a porous medium heat exchanger with liquid film evaporation subjected to a cross-flow of air stream. To solve the problem analytically, we shall idealize the problem as a stagnation point flow of air stream in a porous bed with film evaporation as shown in Fig. 1. In what follows, the mathematically formulation will first be described. A complete solution of heat and mass distribution will subsequently be obtained. Some salient features of the solution and the effects of various parameters on heat and mass transfer will be presented and discussed.

2. Formulation

As shown in Fig. 1, the problem to be considered is a laminar stagnation point flow of air in a porous bed of finite thickness b, with a thin film of liquid water existing at the bottom of the porous bed and above a flat impermeable wall. The impermeable wall is heated at a uniform heat flux q. Assuming that the liquid layer is very thin and stationary, we can place the origin of the coordinate system at the stagnation point above the surface of the liquid layer. The two-dimensional stagnation flow can now be divided into two regions: a plain medium region ($b < y < \infty$) and a porous medium region ($0 < y < b$). The air stream at infinity has a temperature T_∞ and a mass fraction of water vapor w_∞. As the air flow enters the porous bed and is in contact with the liquid film, the temperature of the air will drop and the mass fraction of water vapor will increase due to the evaporation of the thin film. In the plain media region bounded by $b<y<\infty$ (Fig. 1), we have a potential flow so that the solution of the velocity field is $u = kx$ and $v = -ky$ where x and y are the spatial coordinates parallel and normal to the impermeable surface, and u and v the velocity components along the x- and y-directions. The velocity gradient k is the parameter describing the flow strain rate. Under the assumption of constant thermophysical properties and the air and the porous medium is at thermal equilibrium, the governing equations of energy conservation for the moist air stream and species diffusion equation for water vapor are given by

$$-ky\frac{\partial T^+}{\partial y} - \alpha\frac{\partial^2 T^+}{\partial y^2} = 0 \tag{1}$$

$$-ky\frac{\partial w^+}{\partial y} - D\frac{\partial^2 w^+}{\partial y^2} = 0 \tag{2}$$

with the boundary conditions

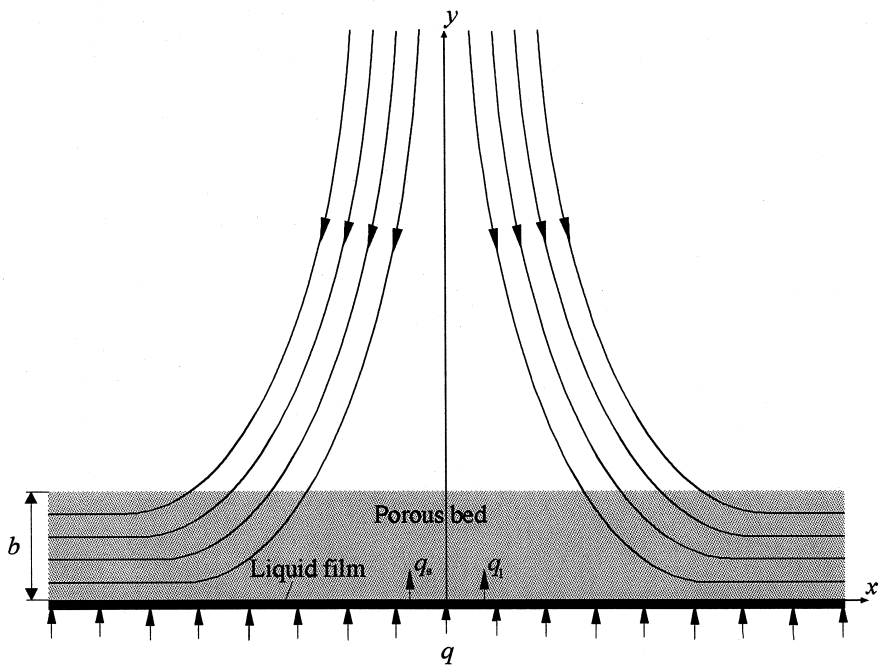

Fig. 1. Schematic defining the problem to be studied.

$$y\to\infty: T^+ = T_\infty; \quad w^+ = w_\infty. \tag{3a,b}$$

In the above, T is the temperature, w the mass fraction of water vapor, α and D the thermal and the mass diffusivities, and the superscripts '+' denote the quantities in the plain media region.

In the porous media region ($0 < y < b$), where the Darcy's law is valid, the macroscopic flow field is again a potential flow with the flow velocity given by (kx/K and $-ky/K$) where K is the permeability of the porous medium. Multiplying the flow velocity by K, we obtain the Darcy's velocity, which can be applied to the conservation equations of energy and mass fraction of water vapor as

$$-ky\frac{\partial T^-}{\partial y} - \alpha_m \frac{\partial^2 T^-}{\partial y^2} = 0 \tag{4}$$

$$-ky\frac{\partial w^-}{\partial y} - D_m \frac{\partial^2 w^-}{\partial y^2} = 0 \tag{5}$$

where the superscripts '−' denote the quantities in the porous medium region; $\alpha_m = \lambda_m/\rho c_p$ is the effective thermal diffusivity with λ_m being the effective thermal conductivity in the porous medium; ρ and c_p are the density and the specific heat of the moist air, and D_m is the effective mass diffusivity in the porous medium which is related to the effective thermal conductivity by

$$Le = \frac{\alpha_m}{D_m} \tag{6}$$

with Le being the Lewis number. In this study, the effective thermal conductivity in the porous medium is evaluated by [14]

$$\frac{\lambda_m}{\lambda} = 1-\sqrt{1-\phi}+\frac{2\sqrt{1-\phi}}{1-C\gamma}\left[\frac{(1-\gamma)C}{(1-C\gamma)^2}\ln\frac{1}{C\gamma} - \frac{C+1}{2} - \frac{C-1}{1-C\gamma}\right] \tag{7}$$

where ϕ is the porosity of the porous bed, $\gamma = \gamma/\gamma_s$ with λ_s being the thermal conductivity of the solid material, and $C = 1.25((1-\phi)/\phi)^{10/9}$ for a packed sphere bed.

The boundary conditions at the gas–liquid interface are

$$y = 0: \quad -\lambda_m \frac{\partial T^-}{\partial y} = q_s; \quad w^- = w_i(T_i, p_\infty) \tag{8a,b}$$

where the sensible heat q_s is related to the latent heat q_l and the total heat flux q applied at the bottom of the liquid layer (see Fig. 1) by

$$q = q_s + q_l \tag{9}$$

with the latent heat q_l being evaluated by [15]

$$q_l = \dot{m}_{v,i} h_{fg} = -\frac{\rho h_{fg} D_m}{1-w_i}\left(\frac{\partial w^-}{\partial y}\right)_{y=0} \tag{10}$$

where $\dot{m}_{v,i}$ is the evaporating flux of water vapor and h_{fg} the latent heat of vaporization. In equation (8b) the relationship between the mass fraction of water vapor w_i at the saturated temperature T_i under the ambient pressure p_∞ can be determined from thermodynamic properties of moist air.

The interfacial conditions between the plain medium and the porous medium are

$$y = b: \quad T^+ = T^-; \quad w^+ = w^-$$

$$\lambda\frac{\partial T^+}{\partial y} = \lambda_m \frac{\partial T^-}{\partial y}; \quad D\frac{\partial w^+}{\partial y} = D_m \frac{\partial w^-}{\partial y}. \tag{11}$$

Because the normal velocity v and all the boundary conditions are independent of x, the solution of the present problem is independent of x so that the term $\partial/\partial x$ does not exist in the above equations. It should be recognized that for the present problem the solutions of temperature and mass fraction of water vapor are coupled through boundary condition (8b).

Introducing the dimensionless quantities

$$Y = y\sqrt{\frac{k}{\alpha_m}} = \frac{y}{b}\sqrt{Pe}; \quad \theta = \frac{T-T_\infty}{(qb/\lambda_m)}; \quad W = \frac{w}{w_\infty}$$

$$\sigma_\alpha = \frac{\alpha_m}{\alpha}; \quad \sigma_D = \frac{D_m}{D}; \quad \sigma_\lambda = \frac{\lambda_m}{\lambda} \tag{12}$$

where $Pe = \sqrt{kb^2/\alpha_m}$ is the Peclet number, the governing equations (1), (2), (4) and (5) can now be nondimensionalized as

$$Y\frac{d\theta^+}{dY} + \frac{1}{\sigma_\alpha}\frac{d^2\theta^+}{\partial Y^2} = 0 \tag{13}$$

$$Y\frac{dW^+}{dY} + \frac{1}{\sigma_D Le}\frac{d^2 W^+}{\partial Y^2} = 0 \tag{14}$$

$$Y\frac{d\theta^-}{dY} + \frac{d^2\theta^-}{\partial Y^2} = 0 \tag{15}$$

$$Y\frac{dW^-}{dY} + \frac{1}{Le}\frac{d^2 W^-}{\partial Y^2} = 0 \tag{16}$$

and the boundary conditions (3), (8) and (11) can be nondimensionlized as

$$Y\to\infty: \quad \theta^+ = 0 \quad W^+ = 1 \tag{17a,b}$$

$$Y = \sqrt{Pe}: \quad \theta^+ = 0^-; \quad W^+ = W^-$$

$$\frac{d\theta^+}{dY} = \sigma_\lambda \frac{d\theta^+}{dY}; \quad \frac{dW^+}{dY} = \sigma_D \frac{dW^-}{dY} \tag{18a–d}$$

$$Y = 0: \quad \frac{\partial\theta^-}{\partial Y} = -\frac{q_s}{q_s\sqrt{Pe}}; \quad W^- = W_i\left(\frac{qb}{\lambda_m}\theta_i + T_\infty, P_\infty\right). \tag{19a,b}$$

Rearranging equation (9) with the aid of equation (10) yields

$$\frac{q_s}{q} = 1 - \frac{q_l}{q}$$

$$= 1 + \frac{w_\infty \sqrt{Pe}}{Ja'(1 - W_i w_\infty)} \left(\frac{dW^-}{dY} \right)_{Y=0} \quad (20)$$

where $Ja' = qb/\rho D_m h_{fg}$ is the modified Jacob number.

Equations (13)–(20) imply that

$$\theta(Y) \text{ or } W(Y) = f(Pe, Le, \sigma_\alpha, \sigma_D, \sigma_\lambda, Ja', T_\infty, w_\infty). \quad (21)$$

3. Analysis

It should be noted that the conservation equations of energy and mass fraction of water vapor, equations (13)–(20), are the second order ordinary differential equations of the form

$$Y \frac{d\Psi}{dY} + A \frac{d^2\Psi}{\partial Y^2} = 0 \quad (22)$$

where A is a constant and Ψ represents θ or W. Equation (22) has a general solution of the form

$$\Psi(Y) = C_1 \sqrt{\pi A} \operatorname{erf}\left(\frac{1}{\sqrt{2A}} Y \right) + C_2 \quad (23)$$

where the error function is defined as

$$\operatorname{erf}(\xi) = \frac{2}{\sqrt{\pi}} \int_0^\xi \exp(-\xi^2) d\xi \quad (24)$$

and C_1 and C_2 are integral constants to be determined by imposing boundary conditions. Solving equations (13) and (15) subject to the appropriate boundary conditions (17)–(19), the dimensionless temperature distributions are

$$\theta^+(Y) = \Lambda_\theta \frac{q_s}{q} 1 - \operatorname{erf}\left(\sqrt{\frac{\sigma_\alpha}{2}} Y \right) \quad (25)$$

$$\theta^-(Y) = -\Lambda_\theta \frac{q_s}{q} \left[\sqrt{\sigma_\alpha}/\Lambda_1 \operatorname{erf}\left(\frac{1}{\sqrt{2}} Y \right) + \Lambda_2 - 1 - \Lambda_3 \sqrt{\sigma_\alpha}/\Lambda_1 \right] \quad (26)$$

where

$$\Lambda_1 = \sigma_\lambda \exp\left[\frac{1}{2} Pe(\sigma_\alpha - 1) \right]; \quad \Lambda_2 = \operatorname{erf}\left(\sqrt{\frac{Pe\sigma_\alpha}{2}} \right)$$

$$\Lambda_3 = \operatorname{erf}\left(\sqrt{\frac{Pe}{2}} \right); \quad \Lambda_\theta = \frac{\Lambda_1}{\sqrt{2Pe}} \left(\sqrt{\frac{\pi}{\sigma_\alpha}} \right). \quad (27)$$

Similarly, the solution of the mass fraction of water vapor can be obtained by solving equations (14) and (16) subjected to the boundary conditions (17)–(19) as follows

$$W^+(Y) = \Lambda_w (W_i - 1) \left[\operatorname{erf}\left(\sqrt{\frac{Le\sigma_D}{2}} Y \right) - 1 \right] + 1 \quad (28)$$

$$W^-(Y) = \frac{\sqrt{\sigma_D}}{\Lambda_4} \Lambda_w (W_i - 1) \operatorname{erf}\left(\sqrt{\frac{Le}{2}} Y \right) + W_i \quad (29)$$

where

$$\Lambda_4 = \sigma_D \exp\left[\frac{LePe}{2} (\sigma_D - 1) \right];$$

$$\Lambda_w = \frac{\sqrt{\pi/Le\sigma_D}}{\Lambda_5 - \sqrt{\pi/Le\sigma_D} - \Lambda_6/\Lambda_4}$$

$$\Lambda_5 = \sqrt{\frac{\pi}{Le\sigma_D}} \operatorname{erf}\left(\sqrt{\frac{PeLe\sigma_D}{2}} \right);$$

$$\Lambda_6 = \sqrt{\frac{\pi}{Le}} \operatorname{erf}\left(\sqrt{\frac{LePe}{2}} \right). \quad (30)$$

Differentiating equation (29) with respect to Y and imposing the resultant expression at $Y = 0$ yields

$$\left(\frac{dW^-}{dY} \right)_{Y=0} = \sqrt{\frac{2Le\sigma_D}{\pi}} \frac{\Lambda_w}{\Lambda_4} (W_i - 1). \quad (31)$$

Substituting equation (31) into equation (20), we obtain

$$\frac{q_s}{q} = 1 + \Lambda_q \frac{W_i - 1}{1 - W_i w_\infty} \quad (32)$$

where

$$\Lambda_q = \frac{w_\infty \sqrt{Pe}}{Ja'} \sqrt{\frac{2Le\sigma_D}{\pi}} \frac{\Lambda_w}{\Lambda_4}. \quad (33)$$

We now obtain the temperature at the gas–liquid interface from equation (26) to give

$$\theta_i = \Lambda_\theta \left[1 + \Lambda_q \frac{W_i - 1}{1 - W_i w_\infty} \right] (\Lambda_2 - 1 - \sqrt{\sigma_\alpha} \Lambda_3/\Lambda_1). \quad (34)$$

Substituting the values of the mass fraction of water vapor W_i at the saturated temperature θ_i into equation (34), we can obtain the gas–liquid interface temperature, and the corresponding W_i.

We now define the Nusselt numbers (Nu_s and Nu_l) owing to the sensible and latent heat transfer as

$$Nu_s = \frac{h_s b}{\lambda_m} = \frac{q_s}{\lambda_m (T_i - T_\infty)} \quad (35)$$

$$Nu_l = \frac{h_l b}{\lambda_m} = \frac{q_l}{\lambda_m (T_i - T_\infty)} \quad (36)$$

where h_s and h_l are the heat transfer coefficient due to sensible and latent heat transfer, respectively. Combing equations (35) and (36) with the aid of equation (9) gives the total Nusselt number Nu as

$$Nu = Nu_s + Nu_l = \frac{hb}{\lambda_m} = \frac{q}{\lambda_m(T_i - T_\infty)} = \frac{1}{\theta_i}. \quad (37)$$

Substituting equation (34) into equation (37) yields

$$Nu = \frac{1}{\Lambda_\theta\left[1 + \Lambda_q \frac{W_i - 1}{1 - W_i w_\infty}\right](\Lambda_2 - 1 - \sqrt{\sigma_\alpha}\Lambda_3/\Lambda_1}. \quad (38)$$

Similarly, the Sherwood number is defined as

$$Sh = \frac{h_D b}{D_m} = \frac{\dot{m}_v b}{D_m \frac{\rho}{1 - w_i}(w_i - w_\infty)} = \frac{-\sqrt{Pe}}{(W_i - 1)}\left(\frac{dW^-}{dY}\right)_{Y=0}. \quad (39)$$

Substituting equation (31) into equation (39), we obtain

$$Sh = -\sqrt{\frac{2PeLe\sigma_D}{\pi}}\frac{\Lambda_w}{\Lambda_4}. \quad (40)$$

4. Results and discussion

As mentioned earlier, there are a total six parameters (Pe, Le, σ_α, σ_λ, σ_D, T_∞, and w_∞) for the problem under consideration. Obviously, a complete parametric study is unrealistic for such a complex problem. For this reason, we shall focus our attention on the characteristics of heat and mass transfer in a stagnation point flow of air through a porous bed made of glass beads. For this specific system, the parameters σ_α, σ_λ, and σ_D will only depend on the porosity ϕ. In the following, the temperature and absolute humidity profiles will first be presented, followed by the discussion of the effects of various parameters on the heat and mass transfer rates.

4.1. Temperature and mass fracture of water vapor profiles

Figure 2 shows the temperature and mass fracture of water vapor profiles at selected porosity: $\phi = 0.15$, 0.4, and 0.85. As shown in Fig. 2a, typically the temperature decreases along the axial Y-direction for each case, indicating heat is transferred from the heated plate to the air stream in the plain medium. It can also be observed that at the interface between the porous medium and the plain medium (i.e. $Y = \sqrt{Pe} = 1$), the slope of each curve in the porous medium is smaller than that in the plain medium because of the higher effective thermal conductivity in the porous medium. As the porosity of the porous medium increases, the liquid–gas interface temperature θ_i increases and the temperature gradient becomes steeper. This is attributed to the fact that the effective thermal conductivity decreases as the porosity increases. The distribution of the mass fracture of water vapor along the axial Y-direction depicted in Fig. 2b shows the same trends as that of temperature. As shown in Fig. 2b, the higher liquid–gas interfacial temperature can result from a higher porosity (or lower thermal conductivity). Therefore, the corresponding mass fracture of water vapor at the liquid–gas interface is higher for larger porosity.

The effects of Lewis number on the mass fracture of water vapor distributions are illustrated in Fig. 3a, which indicates that the gradient of the mass fracture of water vapor within the porous medium becomes flatter as the Lewis number decreases. This is because the mass diffusivity becomes larger as the Lewis number decreases at the same thermal conductivity (or with the same porosity $\phi = 0.4$ for a given porous material). The higher mass transfer rate will lead to a larger latent heat transfer rate or a smaller sensible heat transfer rate. This is why in Fig. 3b, the temperature gradient within the porous medium becomes flatter as the Lewis number decreases.

4.2. Heat transfer and mass transfer rate

It is interesting to investigate the relative importance of the sensible and latent heat exchanges at the liquid–gas interface. Figure 4a presents the variations of the dimensionless latent and sensible heat flux versus the temperature at infinity. It is evident that the heat transfer between the heated plate and the air stream is predominated by the latent heat transfer with $q_l/q > 0.8$. It can also be observed that the latent heat transfer is increased with the increase of the temperature at infinity. This is because more liquid can be evaporated when the incoming air stream has a higher temperature. On the other hand, the higher temperature of the air stream can also lead to the decrease of the sensible heat transfer rate as presented by the dashed line in Fig. 4a. The relative humidity of the air stream also has a significant effect on the performance of the evaporative cooling. This is illustrated in Fig. 4b where the latent and sensible heat flux is plotted against the relative humidity of the air stream. As shown in Fig. 4b, the predominated latent heat flux decreases with the increase of the relative humidity because the potential $(w_i - w_\infty)$ of the mass fracture of water vapor is reduced when the incoming air stream is wet. It may also be noted from Fig. 4b that the sensible heat is increased at a certain degree with the increase of the relative humidity. However, the overall heat transfer rate is reduced for a wet air stream, as shown in Fig. 5a where the Nusselt number versus the relative humidity is presented. This suggests that the evaporative cooling scheme can be directly applied in an air conditioning system in some arid areas. Figure 5b presents the variation of the Nusselt number with the temperature of air at the infinity. It is shown that the overall heat transfer rate is greatly enhanced for the higher environmental temperature.

The influences of the Peclet numbers on the Nusselt number Nu and the Sherwood number Sh for $\phi = 0.4$, $\theta_\infty = 0.43$, and $\varphi = 40\%$ at $Le = 1$ (solid line) and $Le = 2$ (dashed line) are presented in Fig. 6. It is noted

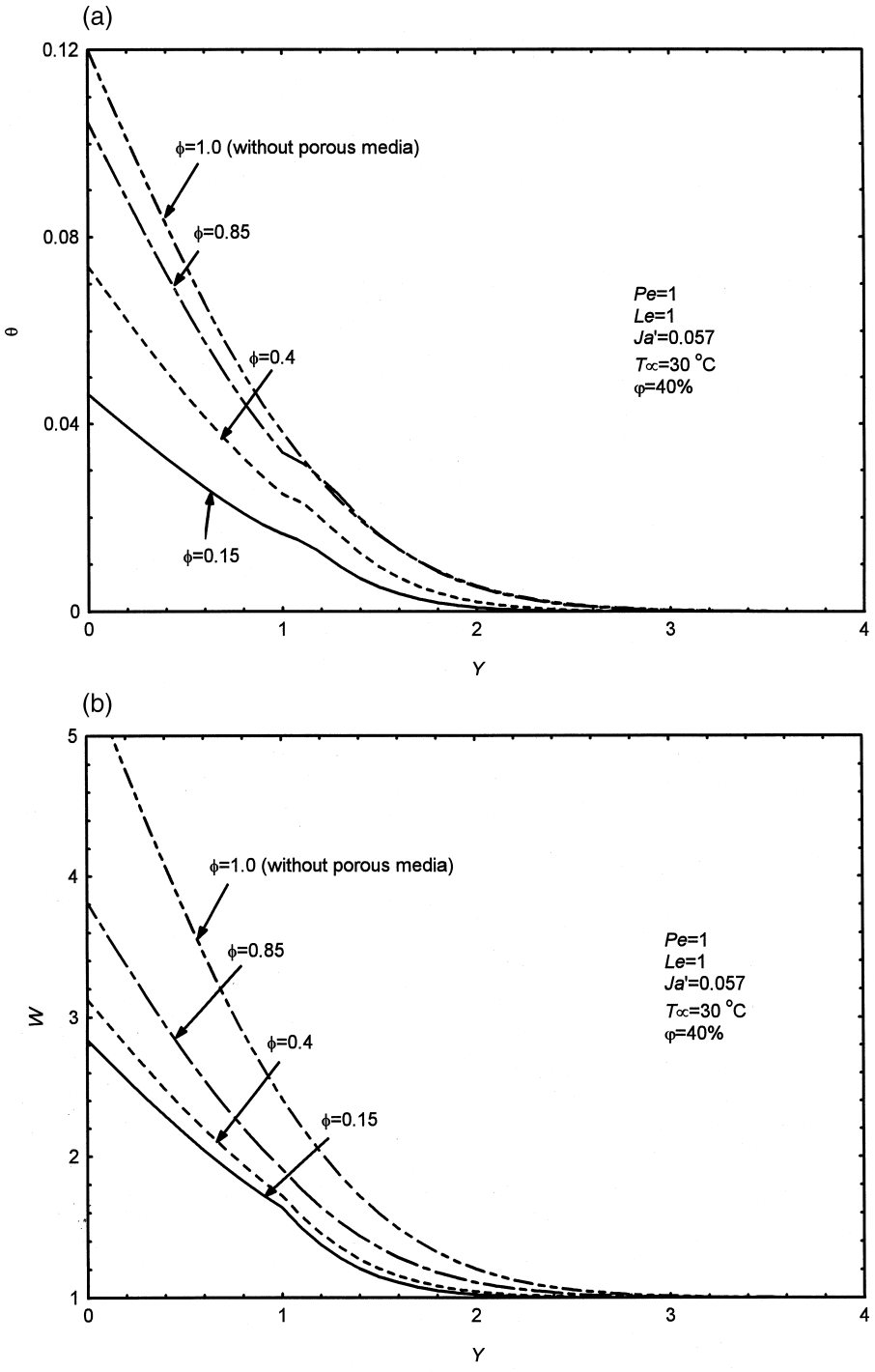

Fig. 2. (a) Typical temperature distribution at $\phi = 0.15$, 0.4, 0.85 and 1 for $Pe = 1$, $Le = 1$, $Ja' = 0.057$, $T_\infty = 30°C$ and $\varphi = 40\%$. (b) Typical mass fraction of water vapor distributions at $\phi = 0.15$, 0.4, 0.85 and 1 for $Pe = 1$, $Le = 1$, $Ja' = 0.057$, $T_\infty = 30°C$ and $\varphi = 40\%$.

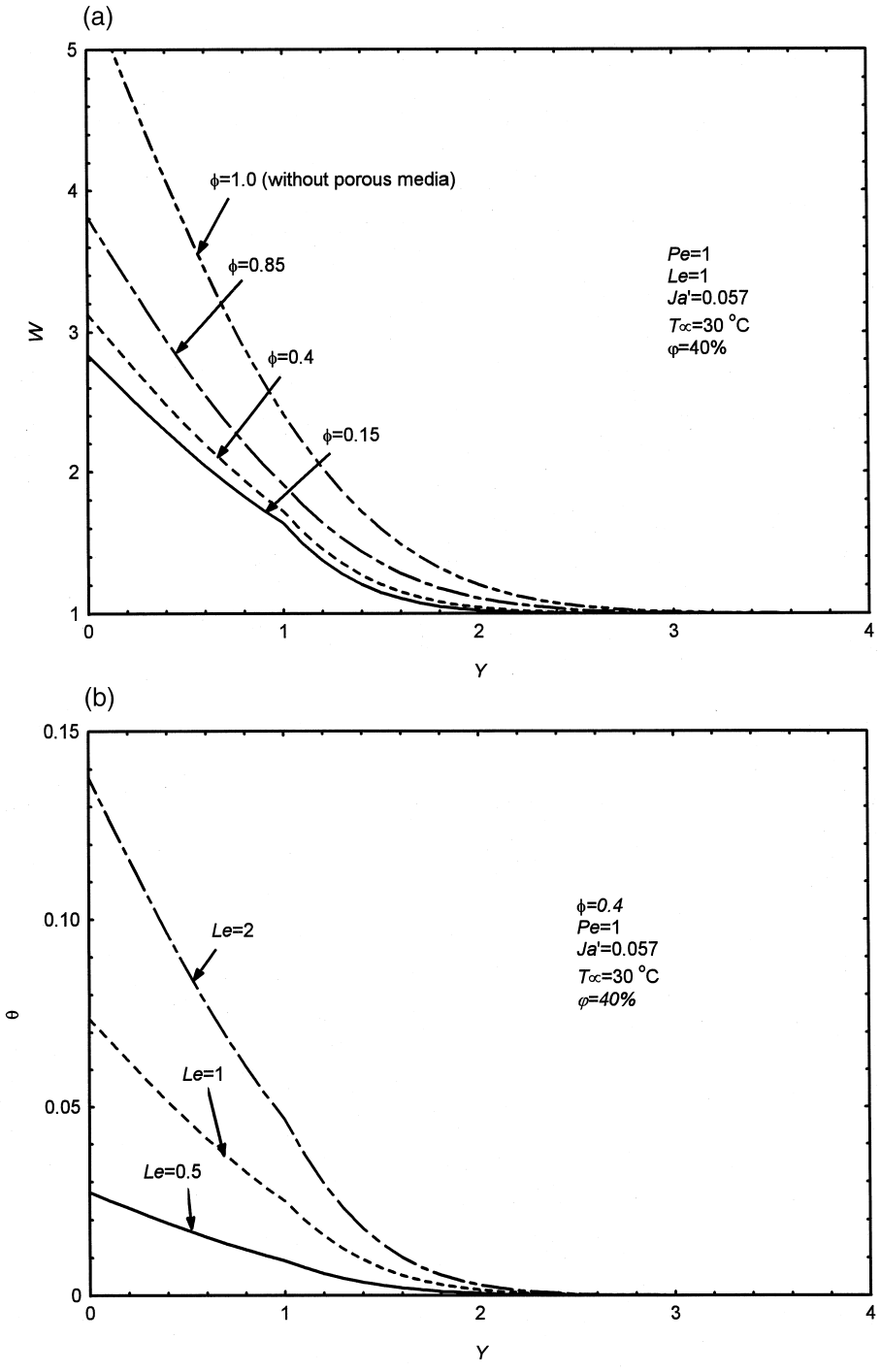

Fig. 3. (a) The effect of Lewis number on the distribution of mass fraction of water vapor at $\phi = 0.4$, $Pe = 1$, $Le = 1$, $Ja' = 0.057$, $T_\infty = 30^\circ C$ and $\varphi = 40\%$. (b) The effect of Lewis number on the distribution of temperature at $\phi = 0.4$, $Pe = 1$, $Le = 1$, $Ja' = 0.057$, $T_\infty = 30^\circ C$ and $\varphi = 40\%$.

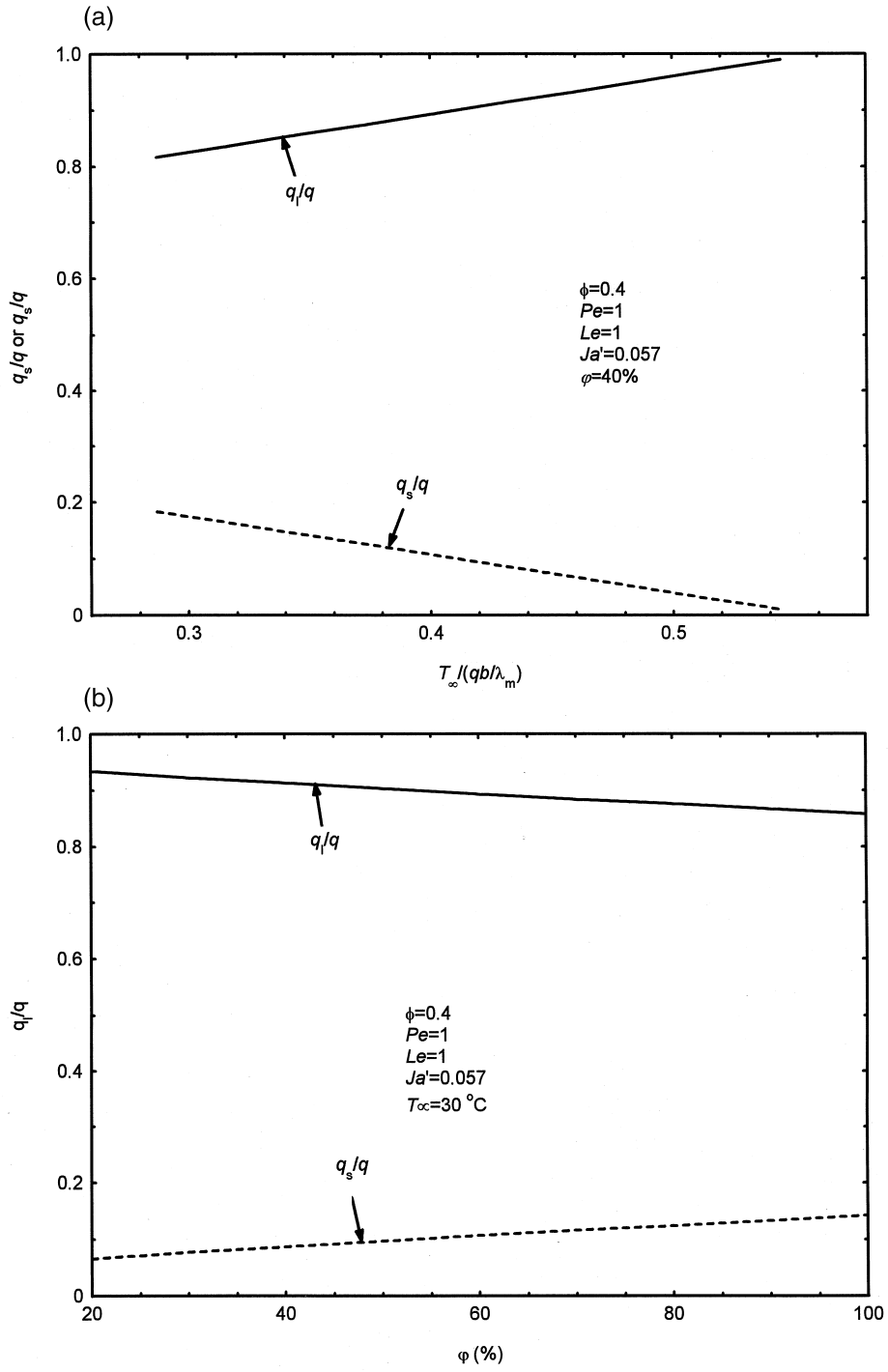

Fig. 4. (a) Variations of latent and sensible heat flux with the ambient temperature at $\phi = 0.4$, $Pe = 1$, $Le = 1$, $Ja' = 0.057$ and $\varphi = 40\%$. (b) Variations of latent and sensible heat flux with the ambient relative humidity at $\phi = 0.4$, $Pe = 1$, $Le = 1$, $Ja' = 0.057$ and $T_\infty = 30^\circ$C.

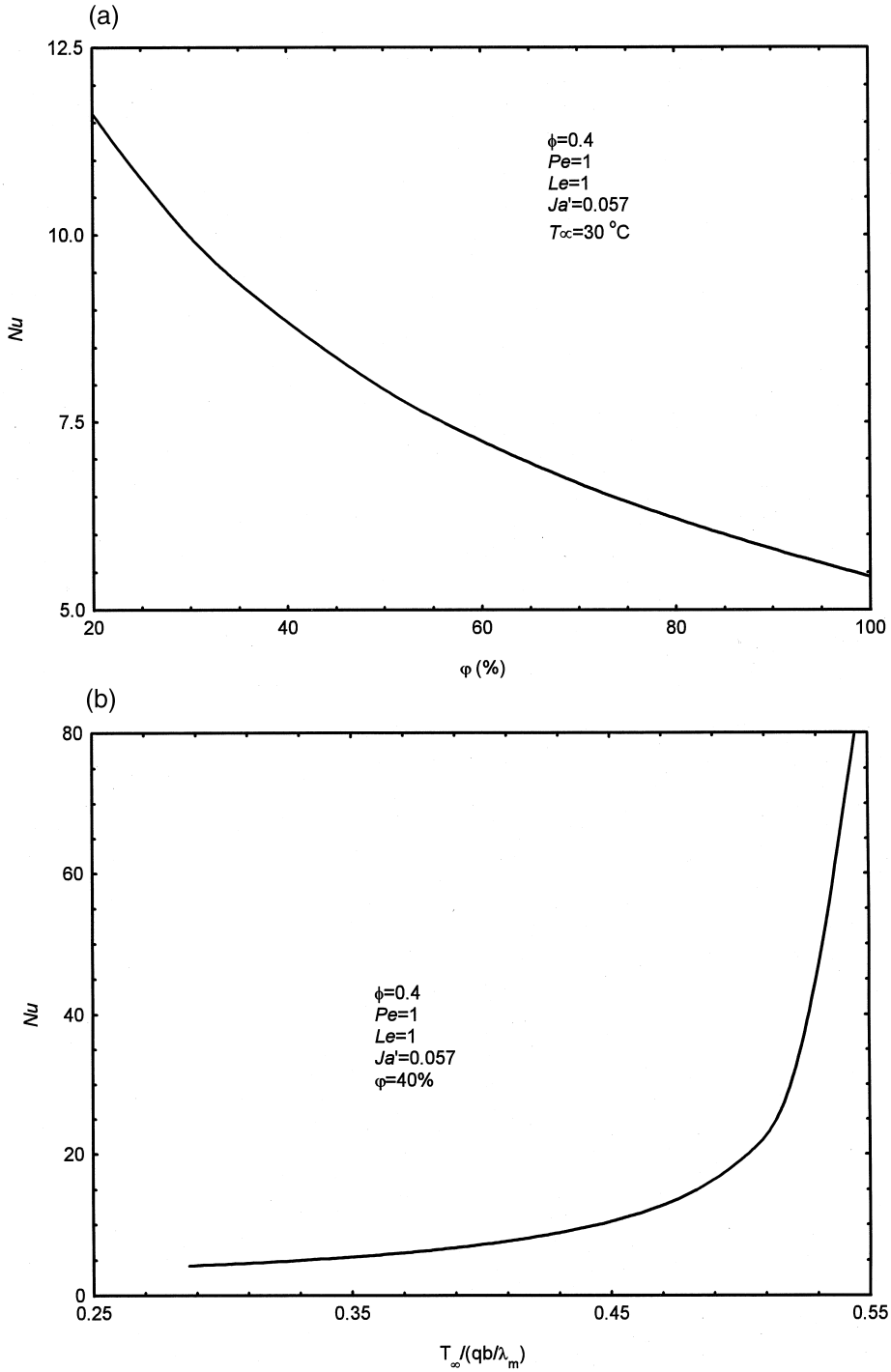

Fig. 5. (a) The effect of the ambient relative humidity on the Nusselt number at $\phi = 0.4$, $Pe = 1$, $Le = 1$, $Ja' = 0.057$ and $T_\infty = 30^\circ C$. (b) The effect of the ambient temperature on the Nusselt number at $\phi = 0.4$, $Pe = 1$, $Le = 1$, $Ja' = 0.057$ and $\varphi = 40\%$.

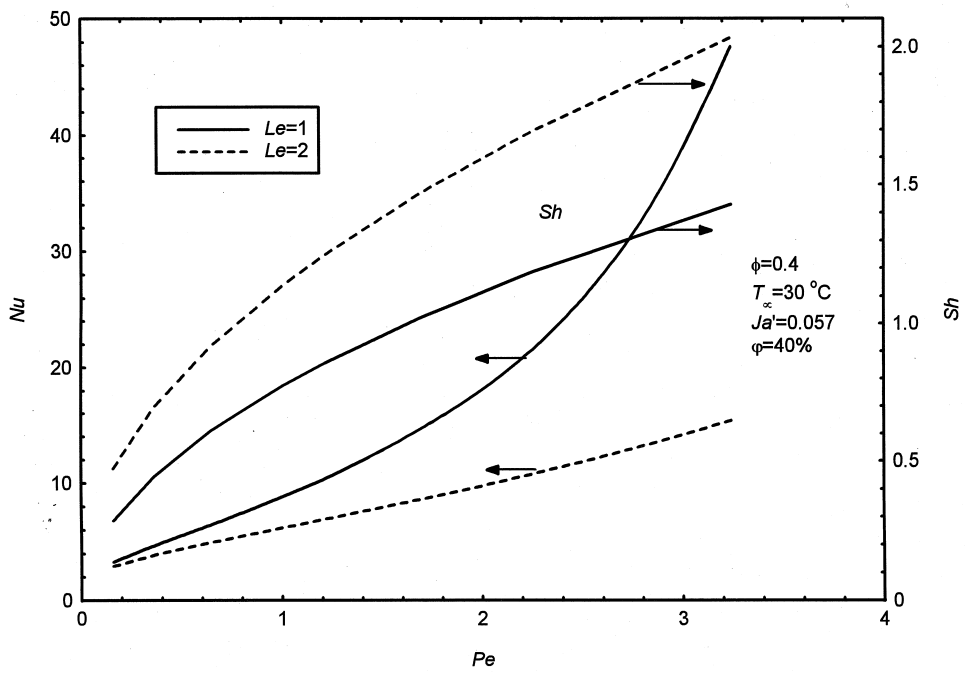

Fig. 6. The effects of the Peclet number and the Lewis number on the Nusselt number and the Sherwood number for $\phi = 0.4$, $Ja' = 0.057$, $T_\infty = 30°C$ and $\varphi = 40\%$.

that both heat and mass transfer rates are increased with the increase of the Peclet number. It is also observed that a larger Lewis number leads to a higher mass transfer rate but smaller heat transfer rate.

5. Concluding remarks

The evaporation of a thin liquid film within a heated porous bed subjected a stagnation flow of air is investigated theoretically. The analysis shows that the coupled heat and mass transfer process in the air stream in a given porous material is governed by the Peclet number Pe, Lewis number Le, the porosity of the porous bed ϕ, as well as the environmental air temperature θ_∞ and relative humidity φ of air. The results show that the heat transfer between the heated plate and the air stream is predominated by the transport of the latent heat in connection with the thin liquid film evaporation. The analysis also demonstrates that a lower relative humidity, a higher temperature of the air stream, and a higher Peclet number lead to an increase of heat transfer rate. For the case when $Le > 1$, the mass transfer rate is enhanced while the heat transfer rate is reduced. These findings are of significance for the design of an indirect evaporative air cooler.

Acknowledgement

This work was supported by Hong Kong RGC Earmarked Research Grant No. HKUST 809/96E.

References

[1] Y.L. Tsay, Analysis of heat and mass transfer in a countercurrent-flow wet surface heat exchanger, International Journal of Heat and Fluid Flow 15 (1994) 149–156.
[2] R.G. Supple, Evaporative cooling for comfort, ASHRAE Journal, 24(8), 1982.
[3] J.L. Peterson, B.D. Hunn, The use of indirect evaporative cooling to reduce peak electric demand in new office buildings, ASHRAE Transaction, 91 (1) (1985).
[4] I.L. Maclaine-Cross, P.J. Banks, A general theory of wet surface heat exchangers and its application to regenerative evaporative cooling, Journal of Heat Transfer 103 (1981) 579–55.
[5] C.F. Kettleborough, C.S. Hsieh, The thermal performance of the wet plastic plate heat exchanger used as an indirect evaporative cooler, Journal of Heat Transfer 105 (1983) 366–373.
[6] C.F. Kettleborough, The thermal performance of the cross-flow indirect evaporative cooler, Proceedings of the

ASME/JSME Thermal Engineering Conference, 1987, pp. 1985–1992.
[7] C.F. Kettleborough, D.G. Waugaman, M. Johnson, The thermal performance of the cross-flow three-dimensional flat plate indirect evaporative cooler, Trans. ASME Journal of Energy Resources Technology 114 (1992) 181–186.
[8] A.T. Wassel, A.F. Mills, Design methodology for a counter-current falling film evaporative condenser, Journal of Heat Transfer 109 (1987) 784–787.
[9] S.T. Hsu, Z. Lavan, Optimization of wet-surface heat exchangers, Energy 14 (1989) 757–770.
[10] P.J. Erens, A.A. Dreyer, Modeling of indirect evaporative air coolers, International Journal of Heat Mass Transfer 36 (1993) 17–26.
[11] D. Pescod, Unit air cooler using plastic heat exchanger with evaporatively cooled plates, Australian Refrigeration, Air Conditioning and Heating 22 (9) (1968) 22–26.
[12] W.-M. Yan, C.-Y. Soong, Convective heat and mass transfer along as inclined heated plate with film evaporation, International Journal of Heat and Mass Transfer 38 (7) (1995) 1261–1269.
[13] W.-M. Yan, Effects of film vaporization on turbulent mixed convection heat and mass transfer in a vertical channel, International Journal of Heat and Mass Transfer 38 (4) (1995) 713–722.
[14] P. Zehner, E.U. Schulunder, Thermal conductivity of granular materials at moderate temperatures (in German), Chemie. Ingr.-Tech. 42 (1970) 933–941.
[15] E.R. Eckert, R.M. Drake, Jr, Analysis of Heat and Mass Transfer, McGraw-Hill, New York, 1972.